# DEFLECTION PREDICTION ON MACHINING THIN-WALLED MONOLITHIC AEROSPACE COMPONENT

## R. Izamshah R.A[1,2], John P.T Mo[1], Songlin Ding[1]

[1]School of Aerospace, Mechanical and Manufacturing Engineering,
RMIT University, Australia

[2]Faculty of Manufacturing Engineering,
Universiti Teknikal Malaysia Melaka, Malaysia

Email: [1]izamshah@utem.edu.my

### ABSTRACT

*Structural titanium alloys are coming in for increased use because they are light, ductile and have good fatigue and corrosion-resistance properties As a result; more manufacturing engineers are learning that machining these alloys can be a tricky job due to their unique physical and chemical properties. The problems are worsened when machining with the low-rigidity part which makes the precision difficult to master. This paper consist of two parts, a new CAD/CAE/CAM integrated methodology for predicting the surface errors when machining a thin-wall low rigidity component and secondly, the statistical analysis to determine the correlation between a criterion variable (form errors) and a combination of a predictor (cutting parameters and component attributes). The proposed model would be an efficient means for analysing the root cause of errors induced during machining of thin-wall parts and provide an input for downstream decision making on error compensation. A set of machining tests have been done in order to validate the accuracy of the model and the results between simulation and experiment were found in a good agreement*

*KEYWORDS: CAD/CAE/CAM, Thin-walled work piece, Titanium alloys, Deflection analysis*

## 1.0    INTRODUCTION

The aerospace industry is the single largest market for titanium products primarily due to the exceptional strength to weight ratio, elevated temperature performance and corrosion resistance. Titanium applications are most significant in jet engine and airframe components that are subject to temperatures up to 1100° F and for other critical structural parts [1]. Usage is widespread in most commercial and military aircraft. Titanium is also used in spacecraft where the many benefits

of titanium are effectively utilized. As new titanium products, alloys and manufacturing methods are employed by the aircraft industry, the use of titanium will expand. Today the use of precision castings and machining technique are making it possible for more complex shaped component to be made in one piece to replace inefficient assembly of part into structures. These components have the characteristics of thin-wall monolithic part which typically being manufacture by machining the features out of one large titanium block.

Thin-wall machining of monolithic parts allows for higher quality and precise parts in less time, impact business issues including inventory and Just-In-Time (JIT) manufacturing. Because of the poor stiffness of thin-wall part, deformation is more likely to occur in the machining of thin-wall part which resulting a dimensional form errors. In current industry practice, the resulting errors are usually compensated through one or more of the following techniques: (i) using a repetitive feeding and final 'float' cut to bring the machined surface within tolerance; (ii) manual calibration to determine 'tolerable' machining conditions; and (iii) a lengthy and expensive trial and error numerical control validation process [2]. Noticeably all of these existing techniques have a tendency to lower productivity. With the forecast of 13,000 new aircraft will be manufacture over the next 20 years, the need for more cost effective manufacturing method for titanium monolithic component is imminent. Therefore, the prediction of resulting surface errors when machining thin-wall monolithic component is crucial in order to increase the part accuracy and productivity.

Accuracy of machined components is one of the most critical considerations for many manufacturers especially in aerospace industry where most of the part used a thin-walled structure. Error comes from deformation of thin-walled during machining and has been largely ignored by CAD/CAM software developers. The strong demand of titanium monolithic component usage has attracting many researchers in this field especially to improve the manufacturing efficiency. Current problems in thin-walled machining are that most of these works were conceptual and considered only parts with a simple geometry such as rectangular plate. This is due to the nature of the limitation in design flexibility to create complex part in FEA software. Alternatively, the complex geometry often been generated from CAD software and transferred to the FEA software with a neutral database form such as IGES, DXF, VDA, STEP and STL. However, owing to the exchanging data of different platform can cause some problems such as loss of data organization, translation inaccuracies, change in number of entities and excessive file size growth. Hence, the need to perform analysis in

same working environment is essential to minimize the possible error when exchanging data and to maintain associativity with the master design. Associativity includes time for remeshing the product model for analysis, the iterative loop of computing forces and deflections. This is not practical when the technique is used on shopfloor.

This paper proposes a new model for predicting the part deflection when machining thin-walled work piece. The paper consist of two parts, first, an integrated CAD/CAE/CAM methodology for predicting the surface errors when machining a thin-wall component and secondly, the statistical analysis to determine the correlation between a criterion variable (part deflection) and a combination of a predictor (cutting parameters and component attributes). The system integration consists of machining load computational model from the machining parameter, feature based geometry model, material removal model, deflection analysis model and NC machining verification model. The proposed CAD/CAE/CAM methodology is implemented with CATIA V5 platform using the Mechanical Design workbench, Generative Structural Analysis workbench, Advanced Meshing workbench and Machining workbench.

## 2.0    LITERATURE REVIEW

There were few reported work been done in predicting the deformation of thin-wall part. Budak and Altintas [3] used the beam theory to analyse the form errors when milling using slender helical endmill for peripheral milling of a cantilever plate structure. The slender helical endmill is divided into a set of equal element to calculate the form errors acting by the cutting forces on both tool and the workpiece. Kline *et.al.* [4] used a thin-wall rectangular plate element model clamped on three edges. He used an equivalent concentrated force to calculate the deflection of the tool and the work piece. The form errors are obtained by summing the tool and the work piece deflection. The effects of workpiece and cutter dynamic deflections on the chip load are proposed by Elbastawi and Sagherian [4]. Included in their model is the tracking of the changing of dynamics stiffness of workpiece geometry. In addition, the effects of cutter deflection for estimating the instantaneous uncut chip thickness were proposed by Sutherland and Devor [5]. Later, Tsai and Liao [6] developed an iteration schemes to predict the cutting forces and form error on thin-wall rectangle plate. The cutting force distribution and the cutting system deflections are solved iteratively by modified Newton-Raphson method. Ratchev *et.al.* [7] investigated the modelling and simulation environment

for machining low-rigidity components. Later in his work, Ratchev *et.al.* [8] modelled the material removal process using voxel-based representations by cutting through the voxels at the tool/part contact surface and replacing them with equivalent set of mesh. He used Aluminium Alloys 6082 for the experimental analysis and verification. Rai and Xirouchakis [9] consider the effects of fixturing, operation sequence and tool path in transient thermo-mechanical coupled milling simulation of thin-walled components. Recently, Izamshah *et.al.* [10] adopted the Lagrangian method in his machining simulation, in which each individual node of the mesh follows the corresponding material particle during motion. The workpiece is modelled as a plastic object so that the material can be deform and cut by the endmill teeth.

Despite of several significant works on modelling thin-wall machining that has been developed, there still a requirement for more efficient approach on modelling the thin-wall machining especially for minimizing the analysis time from initial part creation to analysis result. The advantages of the proposed model over previous work are the integration between CAD/CAE/CAM, fast design-analysis loop and the flexibility to create complex finite element models while maintaining associativity with the master design, thereby avoiding time-consuming and error-prone transfer of geometry.

### 3.0 MODELLING AND SIMULATION SYSTEM ARCHITECTURE

The proposed modelling and simulation system architecture for machining thin-wall components is shown in Figure 1. The system consist of several model, namely, machining load computational model derived from the machining parameter, feature based geometry model, material removal model, deflection analysis model and NC machining verification model. The methodology is performed within the CAD environment and the analysis model is fully associative with the CAD geometry and specification. MATLAB software was used in machining load computational model while others models were implemented using CatiaV5 software using Mechanical Design workbench, Advanced Meshing workbench and Generative Structural Analysis workbench. The simulation is perform by automate the task for modelling solids object, material removal and structural analysis with CatiaV5 through the use of macros, with Windows as the operating system and Visual Basic as the programming language In addition multiple regression technique is used to perform the statistical analysis to determine the correlation between a criterion variable; part deflection

and a combination of predictor variables. Finally, both models were validating with a set of machining tests. The methodology consists of several procedures with different functions as follows:

## Machining load computational model

In the machining load computational model, the machining parameters and tool geometry, namely, cutting speed (rpm), radial depth of cut, axial depth of cut, feed rate (mmpt), tool diameter, helix angle ($\beta$) and specific cutting forces (Kt and Kr) are used as an input to calculate the machining loads. The procedure to calculate the machining load is described later in Section 3.1. The calculated machining loads is stored and saved in a native *ASCII file* format and will be used as an input in the deflection analysis model.
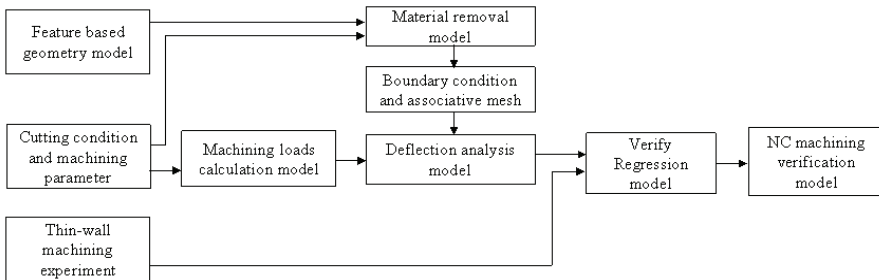


FIGURE 1: Modelling and simulation system architecture.

## Feature based geometry model

The component feature attributes such as the initial workpiece dimensions and material properties are created in the Catia Mechanical Design workbench. The part is created by automating the task for modelling solids object with Catia V5 through the use of macros, with Windows as the operating system and Visual Basic as the programming language. By using a simple form the dimension are enter which define the geometry of the part (length, thickness and height). This application automatically and immediately creates the part compare with the manual process that would require construction of lines and generation of solid model. The created component is saved in *CATPart* file format and work as a master design. Any changes and update of material removal need to be done in this master design.

## Material removal model

To model the material removal process during machining, the cutter shape and the cutter path that is coincidence with the workpiece

material will be remove using extrude (cut) and array function in the Catia Mechanical Design workbench as shown in Figure. 2. For the first step, the cutter is set at the entry of the workpiece and the material which is coincidence with the cutter shape are remove and saved as a new *CATPart* file. Once the cutter feed position is defined, the component feature will be input to Catia Advanced Meshing Tool workbench for generation of associative mesh for the solid component. At this stage, global parameters such as the shape and the size of the elements needs to be specify to perform the finite element analysis. Deflection analysis model

Catia Generative Structural Analysis workbench are use to perform a static analysis for part deflection prediction. At this phase analysis information such as nodes, elements, material properties, boundary conditions and the calculated machining load will be input to calculate the deflection. The procedure to calculate the part deflection is described later in Section 3.2. The FEA results which contain the elements and nodes values is stored and saved in a native *ASCII file* format and saved in *CATAnalysis file* and stored in a knowledge-based template. The cutter feed position is then move to the next position and the material on the new feed step will be removed to perform the subsequent analysis. Finally, after repeating this procedure at different location along the feed direction, the complete surface form errors of the component are obtained and are used in Catia Machining workbench for tool path compensation and NC verification.

## NC machining verification model

Once the complete surface form errors of the thin-wall are obtain, the tool paths can be corrected to compensate for machining error. The compensation is done by mirroring the surface error in the opposite direction of the wall deflection along the feed direction. On the other hand, the tool needs to be tilt following the compensated curve along the feed direction. The compensated tool path, which contains the coordinate values are transfer to the Catia Machining workbench to generate the NC codes.
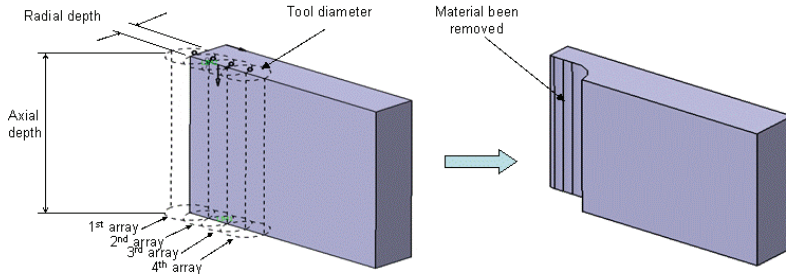
FIGURE 2: CAD based material removal model for machining.

## 3.1 Machining load model for helical endmill

As shown in Figure 3, the machining loads acting on a helical flute endmill are equally discretized into a finite number of elements along the tool axis. The total cutting loads ($F_x$, $F_y$ and $F_z$) acting on the tool at a particular instant are obtain by summing the force components acting on each individual discretized element [16, 17, 18].
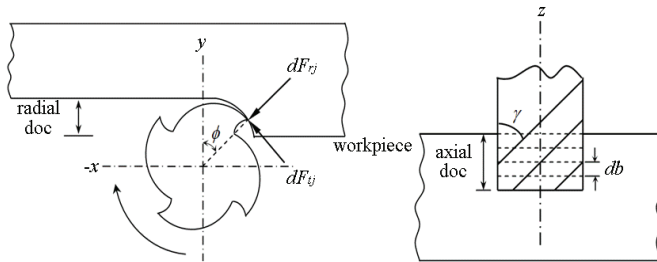


FIGURE 3: Cutting force model for helical endmill.

$$dF_{tj}(\phi, z) = [K_{tc}h_j(\phi, z) + K_{te}]\,dz\,,$$
$$dF_{rj}(\phi, z) = [K_{rc}h_j(\phi, z) + K_{re}]\,dz\,,$$
$$dF_{aj}(\phi, z) = [K_{ac}h_j(\phi, z) + K_{ae}]\,dz \tag{1}$$

where $dF_{tj}$, $dF_{rj}$ and $dF_{aj}$ are differential forces corresponding to discretized element thickness in the tangential, radial and axial directions. The coefficients $K_{tc}$, $K_{rc}$, $K_{ac}$ and $K_{te}$, $K_{re}$, $K_{ae}$ are the specific cutting force coefficients and specific edge cutting force coefficients to each tangential, radial and axial direction, determined from the experimental analysis. $\phi$ is the tool's immersion angle start from positive y-axis and $h_j$ is the instantaneous uncut chip thickness for the flute $j$ and can be define as:

$$h_j(\phi, z) = f_t \sin\phi(z) \tag{2}$$

where $f_t$ is the feed per tooth and $\phi(z)$ is the entry and exit angle for flute $j$ at certain position in the axial direction. Since this study using a helical cutter the full length of the cutting edge does not enter (or exit) the cut at the same instant and the angular delay between disretize elements $\chi$ can be approximated as follows:
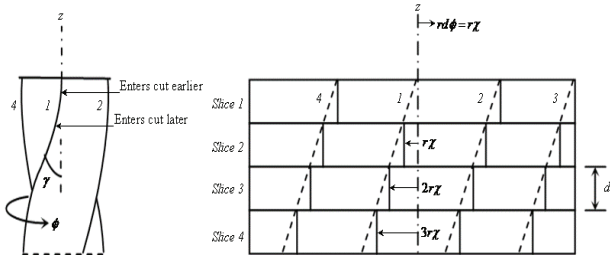


FIGURE 4: Discretized unrolled helical endmill geometry.

$$\chi = \frac{db\tan(\gamma)}{r}(rad) \tag{3}$$

where r is the tool diameter, $\gamma$ is helix angle and db is the element thickness. Rearranging Eqs. (3) and substituting $d\phi$ for $\chi$ yields:

$$db = \frac{r.d\phi}{\tan(\gamma)} \tag{4}$$

By substituting and integrating the differential cutting forces from Eqs. (1) to (4) within the lower and upper boundaries of the flute which is in cut. The tangential, radial and axial forces can be transformed in $x$, $y$, $z$ Cartesian directions and becomes:

$$F_{xj}(\phi) = -\frac{K_t f_t r}{4\tan\gamma}\left[-\cos 2\phi + K_r(2\phi(z) - \sin 2\phi(z))\right]_{Zjl(\phi)}^{Zju(\phi)}$$

$$F_{yj}(\phi) = -\frac{K_t f_t r}{4\tan\gamma}\left[2\phi(z) - \sin 2\phi(z) + K_r\cos 2\phi(z)\right]_{Zjl(\phi)}^{Zju(\phi)}$$

$$F_{zj}(\phi) = -\frac{K_a K_t f_t r}{\tan\gamma}\left[\cos\phi(z)\right]_{Zjl(\phi)}^{Zju(\phi)} \tag{5}$$

where $Zjl(\phi)$ and $Zju(\phi)$ are the lower and upper axial engagement limits of the in cut immersion of the flute $j$. From Eqs. (5) the instantaneous cutting forces acting on the whole endmill can be obtained, which are used as the input for fea to compute the deflection of the workpiece.

## 3.2 Finite element modelling of thin-wall workpiece

The structural of the thin-wall workpiece is modelled with the three-dimensional twenty-node parabolic hexahedron solid element as shown in Figure 5. Parabolic hexahedron solid element is preferred since the thickness of the wall is very thin and the change in structural properties of the wall due to material removed is very important for accurate prediction of the wall deflections [16, 17]. For the three-dimensional element, each node has three degrees of freedom, i.e, three displacements ($\delta_x$, $\delta_y$ and $\delta_z$) and the displacements within each element are interpolated by the nodal values [18].
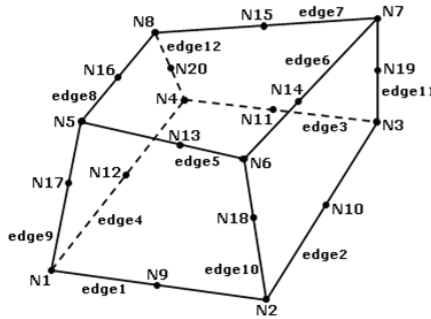


FIGURE 5: Parabolic hexahedron solid element.

Figure 6 shows the thin-wall component model for deflection calculations. The initial wall thickness $t_i$ is reduced to $t_c$ at the transient zone where the cutter flutes enter and exit the material in the milling process. The displacements of the whole structure component are obtained by assembling and solving the finite element equations for each element together as follows:

$$\left[K_{wp}\right]_{nwp \times nwp} \left\{\delta\right\}_{nwp \times 1} = \left\{F\right\}_{nwp \times 1} \tag{6}$$

where $\left[K_{wp}\right]_{nwp \times nwp}$ is the stiffness matrix of the workpiece, $\left\{\delta\right\}_{nwp \times 1}$ is the nodal displacement of the workpiece and $\left\{F\right\}_{nwp \times 1}$ is the vector of the cutting force acting on the transient surface of the workpiece calculated in Section 3.1. The nodal displacement for the structural component can be solved by defining the displacement boundary conditions for the model.
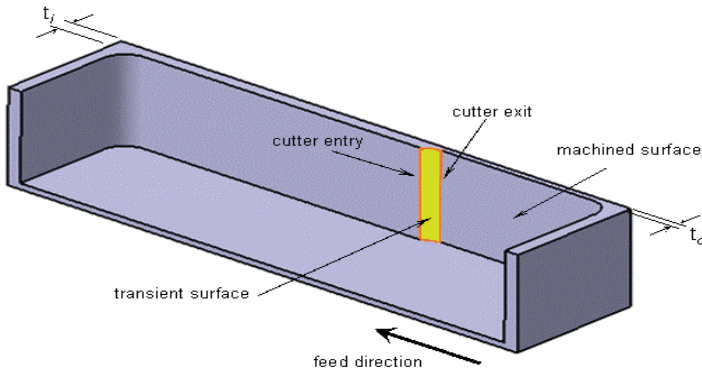
Figure 6: Modelling the thin-wall component.

## 3.3     Statistical analysis

Multiple regression technique is used to perform the statistical analysis to determine the correlation between a criterion variable; part deflection and a combination of a predictor variables namely speed, feed rate, radial depth of cut, wall thickness, wall height and wall length. It can be used to analyse data from any of the major quantitative research designs such as causal-comparative, correctional and experimental. This method is also able to handle interval, ordinal, or categorical data and provide estimates both of the magnitude and statistical significance of the relationship between variables [15]. The multiple regression models can be expressed as:

$$y_{D1, D2, D3, D4, D5} = \beta_0 + \beta_S S + \beta_F F + \beta_{RDOC}RDOC + \beta_{WPT}WPT + \beta_{WPH}WPH + \beta_{WPL}WPL \qquad (7)$$

where

$y$ = displacement (μm) at $D1$, $D2$, $D3$, $D4$ and $D5$
$S$ = Speed (rpm)
$F$ = Feed rate (mmpt)
$RDOC$   = Radial depth of cut (mm)
$WPT$     = Workpiece thickness (mm)
$WPH$    = Workpiece height (mm)
$WPL$    = Workpiece length (mm)

The general null hypotheses was described as the effects of speed, feed rate, radial depth of cut, workpiece thickness, workpiece height and workpiece length on displacement do not significantly differ from zero. The null hypotheses and alternative hypotheses can be written as:

$$H_o = \beta_S = \beta_F = \beta_{RDOC} = \beta_{WPT} = \beta_{WPH} = \beta_{WPL} = 0$$
$$H_a = \text{at least one of the } \beta \text{ does not equal to zero}$$

The regression analysis is verified by using the residual plot graph, which shows the residuals on the vertical axis and the independent variable on the horizontal axis. If the points in a residual plot are randomly dispersed around the horizontal axis, a linear regression model is appropriate for the data; otherwise, a non-linear model is more appropriate.

## 4.0    NUMERICAL AND EXPERIMENTAL WORK

The proposed CAD/CAE/CAM integrated methodology for minimizing the surface errors when machining a thin-wall low rigidity component was experimentally tested by comparing the simulation results with the results of experiment for an identical set of test components. The geometry of the component used in the simulation and experiment is shown in Figure 7. Twenty-node parabolic hexahedron solid element is used to discretized the component for FE model. Only the bottom face of the component is clamped and the other four sides are free. The authors have tested three uniform finite element meshes for the component wall, 100x1x10, 200x2x20 and 300x4x40 (number of elements in X-direction) x (number of elements in Y-direction) x (number of elements in Z-direction), the numerical results for the 200x2x20 and 300x4x40 meshes were being very close. Hence, 200x2x20 is adopted as the finite element mesh to save the computational time. The component was predicted and measured at 30 equally space at one side of the wall along the feed direction. The radial depth of cut is 0.3 mm and the axial depth of cut is 15 mm.
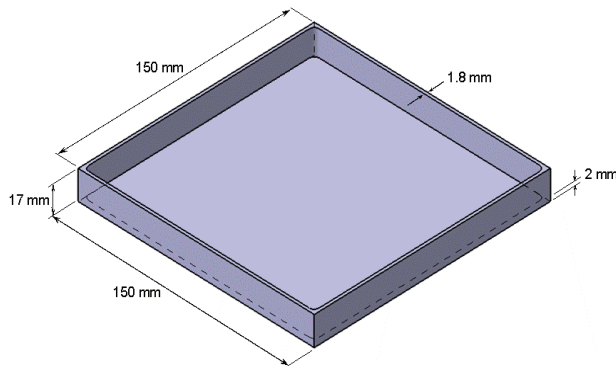


FIGURE 7: Work piece dimension for simulation and experimental.

The experimental set-up is shown in Figure 8. All experimental tests were performed on a HAAS VF1 vertical machining center. Three component Kistler dynamometer (type 9257B) and Kistler charge amplifier (type 5070A) are used to measure the cutting loads, while National Instrument DAQ card is used to acquire the signal. The wall deflection is measured using three Lion Precision ECL 130 inductive displacement sensors. The sensors are mounted at three different equal locations (37.5, 75 and 112.5 mm) at the back of the workpiece. Both the signals from the dynamometer and displacement sensors are then been analyse using LabVIEW 8.5.1.
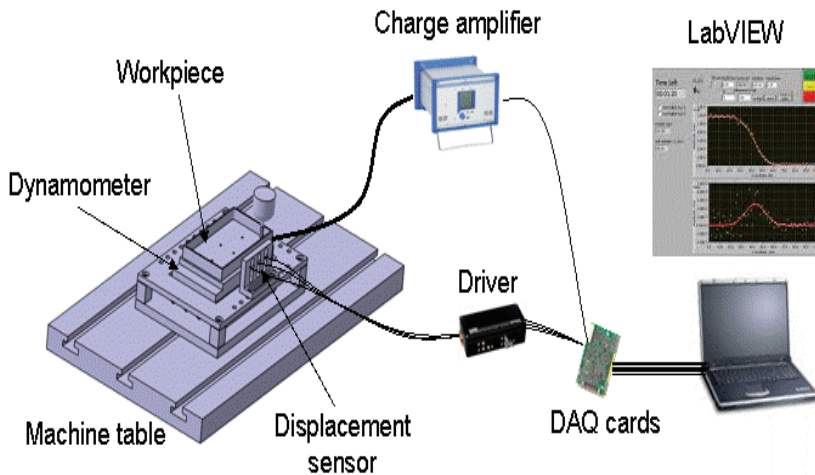


FIGURE 8: Experimental set-up

The workpiece material used in the simulation and experimental is annealed alpha-beta titanium alloy, Ti-6Al-4V. The chemical composition and mechanical properties of the material is shown in Table 1 and 2, respectively. Table 3 shows the specification of carbide flat end mills used in the experiment. To perform the multiple regression analysis, a set of 27 runs on titanium alloys were generated from Section 3.2. The cutting parameters data were obtained from the industrial partner Production Parts Pty. Ltd. Australia, for finishing cycle on machining titanium alloys material. Table 4 shows the 6-Factors 3-Level design of experiment for the multiple regression analysis. The criterion variable are calculated at five different location along the workpiece feed direction (i.e. D1=0, D2=1/4*WPL*, D3=1/2*WPL*, D4=3/4*WPL* and D5=*WPL*). A commercial statistical package SPSS 17.0 was used to do the regression analysis.

TABLE 1: Chemical compositions of Ti-6Al-4V alloy (wt. %)

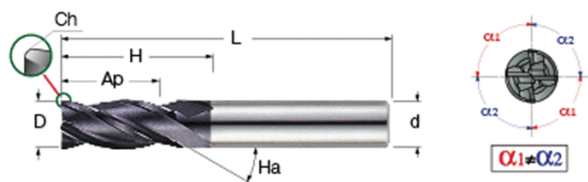| Chemistry | N | C | H | O | Fe | Al | V | Ti | Other elements |
|---|---|---|---|---|---|---|---|---|---|
| % w/w, min. | - | - | - | - | - | 5.50 | 3.50 | - | - |
| % w/w, max. | 0.05 | 0.10 | 0.0125 | 0.20 | 0.30 | 6.75 | 4.50 | Balance | 0.40 |

TABLE 2: Mechanical properties of Ti-6Al-4V alloy at room temperature.

| Density [kg/m$^3$] | Young's modulus [GPa] | Poisson ratio | Yield strength [MPa] | Hardness [HB] | Elongation [%] |
|---|---|---|---|---|---|
| 4430 | 113.8 | 0.34 | 880 | 334 | 14 |

TABLE 3: Cutting tool specification.



| D | d | Ap | H | L | Flute | Ha° | Rd° | Shank | Ch |
|---|---|---|---|---|---|---|---|---|---|
| 6.00 | 6.00 | 14.00 | 20.00 | 57.00 | 4 | 38.0 | 5.0 | C | 0.25X45 |

TABLE 4: Design of experiment for the multiple regression analysis.

| | Level 1 | Level 2 | Level 3 |
|---|---|---|---|
| Speed (rpm) | 4244 | 4509 | 4774 |
| Feed rate (mmpt) | 0.02 | 0.05 | 0.08 |
| Radial depth of cut (mm) | 0.1 | 0.2 | 0.3 |
| WP Thickness (mm) | 1.5 | 2 | 2.5 |
| WP Height (mm) | 5 | 10 | 15 |
| WP Length (mm) | 60 | 90 | 120 |

## 5.0    CUTTING LOADS VALIDATION

MATLAB 7.7 was used for the machining loads computational as described in Section 3.1. To validate the cutting loads model, the predicted forces are compared with measured forces for finishing cycle. As in Section 3.1, the milling forces can be transformed in $x$, $y$ and $z$. However, for the case of thin-wall machining, the force acting in the opposite direction of the wall is specifically considered as it has major impact on the wall deflection, which in this case is $F_y$. The wall thickness is to be reduced from 1.8 mm to 1.5 mm with 3500 rpm spindle speed and a feed rate of 0.05 mm feed per tooth which is constant along the feed direction. Others machining parameters are wall height is 17 mm, axial depth of cut is 15 mm, radial depth of cut is 0.3 mm and the work

piece material is titanium alloys. Figure 9 shows the instantaneous predicted and measured force $F_y$ for one cutter revolution. As it can be clearly observed, both the values between predicted and measured force are in a good agreement. The calculated machining loads will be use as an input for the FEA to calculate the deflection of the work piece during machining.
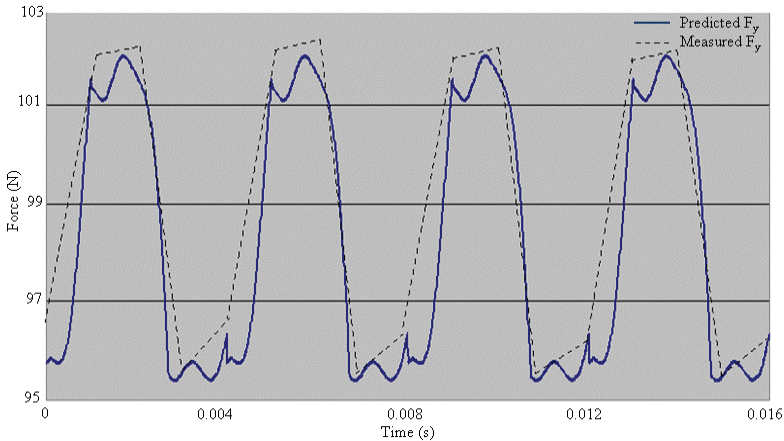


FIGURE 9: Calculated cutting force for one cutter revolution.

## 5.1    Part deflection validation

Figure 10 shows the displacement values for three sensors between simulation and experiment. The cutter feed step is set at 30 equally space location at one side of the wall along the feed direction. The material from the previous feed step need to be removed once the cutter move to the next feed step. Table 5 shows the errors calculation between predicted and measured value. It can be seen that both the displacement obtained by simulation closely match the displacement that are obtained by experiment. The agreement value between predicted and measured is between 80.3% and 99.9%. Figure 11 shows the simulation result of the displacement magnitudes at the middle location of cutter feed step. From the cut plane analysis of the wall, it shows that the form errors are smallest at the bottom of the part. The form errors magnitudes increase towards the middle of the part and decrease towards the end of the part, where the wall flexibility decreases. Due to the decreasing stiffness of the wall as a result of material removal, there is an increasing value of form errors between two regions (start and end) in the feed direction. To a large extent, the more flexible the wall, the higher surface errors result during cutting. Once the deflection of the work piece is established, the tool path is optimised by recalculating the coordinates of the cutter. To compensate

the resulting profile error, the cutter location needs to be modified from the initial position to the compensated position by a distance of the resulting displacement value at certain cutter feed position.
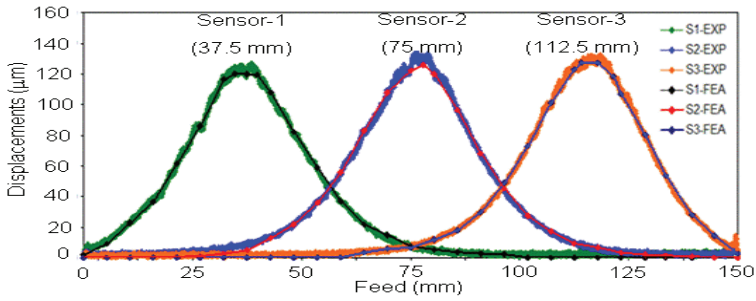


FIGURE 10: Comparison between simulation and experiment of displacement along the workpiece length.

TABLE 5: Error calculations between prediction and measured value.

| Feed (mm) | S1 | | | S2 | | | S3 | | |
|---|---|---|---|---|---|---|---|---|---|
| | FEA | EXP | Agreement | FEA | EXP | Agreement | FEA | EXP | Agreement |
| 0 | 1.839 | 1.701 | 91.9 | 0.001 | 0.001 | 87.1 | 1.82E-04 | 1.98E-04 | 91.8 |
| 5 | 9.135 | 9.880 | 92.5 | 0.006 | 0.007 | 88.5 | 3.96E-04 | 3.37E-04 | 82.5 |
| 10 | 22.841 | 23.164 | 98.6 | 0.044 | 0.050 | 88.1 | 1.94E-03 | 1.67E-03 | 83.8 |
| 15 | 36.505 | 37.627 | 97.0 | 0.175 | 0.208 | 84.1 | 3.56E-03 | 3.96E-03 | 89.9 |
| 20 | 61.598 | 61.419 | 99.7 | 0.427 | 0.362 | 82.0 | 6.29E-03 | 6.77E-03 | 92.9 |
| 25 | 86.071 | 85.222 | 99.0 | 1.016 | 1.201 | 84.6 | 1.01E-02 | 1.12E-02 | 89.9 |
| 30 | 116.508 | 116.029 | 99.6 | 2.625 | 3.035 | 86.5 | 1.45E-02 | 1.51E-02 | 96.3 |
| 35 | 119.971 | 121.016 | 99.1 | 5.014 | 5.676 | 88.3 | 1.78E-02 | 1.72E-02 | 96.4 |
| 40 | 107.952 | 107.357 | 99.4 | 12.702 | 13.234 | 96.0 | 1.97E-02 | 1.72E-02 | 85.5 |
| 45 | 82.116 | 81.632 | 99.4 | 21.805 | 22.047 | 98.9 | 2.20E-02 | 2.22E-02 | 98.8 |
| 50 | 58.810 | 58.456 | 99.4 | 35.995 | 36.286 | 99.2 | 0.118 | 0.147 | 80.3 |
| 55 | 36.920 | 37.285 | 99.0 | 55.582 | 55.121 | 99.2 | 0.259 | 0.312 | 83.0 |
| 60 | 21.694 | 21.642 | 99.8 | 82.868 | 82.075 | 99.0 | 3.415 | 3.594 | 95.0 |
| 65 | 14.727 | 14.155 | 96.0 | 108.051 | 107.861 | 99.8 | 5.909 | 6.051 | 97.7 |
| 70 | 7.608 | 7.816 | 97.3 | 120.119 | 123.653 | 97.1 | 6.603 | 6.731 | 98.1 |
| 75 | 5.280 | 5.156 | 97.6 | 120.017 | 121.749 | 98.6 | 11.757 | 11.940 | 98.5 |
| 80 | 3.654 | 3.724 | 98.1 | 96.585 | 95.843 | 99.2 | 17.924 | 18.047 | 99.3 |
| 85 | 2.750 | 2.798 | 98.3 | 68.106 | 67.111 | 98.5 | 29.754 | 29.788 | 99.9 |
| 90 | 2.291 | 2.153 | 93.6 | 45.251 | 44.592 | 98.5 | 48.877 | 48.023 | 98.2 |
| 95 | 3.35E-02 | 3.49E-02 | 95.9 | 27.389 | 27.602 | 99.2 | 72.829 | 72.790 | 99.9 |
| 100 | 2.68E-03 | 2.82E-03 | 95.1 | 17.132 | 17.359 | 98.7 | 101.257 | 100.619 | 99.4 |
| 105 | 1.25E-03 | 1.41E-03 | 88.7 | 9.381 | 9.656 | 97.2 | 119.910 | 122.700 | 97.7 |
| 110 | 1.22E-03 | 1.24E-03 | 98.4 | 6.644 | 6.908 | 96.2 | 119.689 | 122.300 | 97.9 |
| 115 | 9.34E-04 | 9.53E-04 | 98.0 | 3.392 | 3.487 | 97.3 | 107.051 | 107.523 | 99.6 |
| 120 | 6.18E-04 | 6.86E-04 | 90.1 | 2.043 | 2.002 | 98.0 | 80.345 | 80.461 | 99.9 |
| 125 | 3.72E-04 | 3.96E-04 | 93.9 | 1.493 | 1.583 | 94.3 | 53.641 | 53.071 | 98.9 |
| 130 | 1.97E-04 | 2.02E-04 | 97.5 | 0.906 | 1.109 | 81.7 | 27.968 | 28.422 | 98.4 |
| 135 | 1.82E-04 | 1.90E-04 | 95.8 | 0.015 | 0.013 | 90.3 | 14.252 | 14.131 | 99.1 |
| 140 | 1.78E-04 | 1.81E-04 | 98.3 | 0.003 | 0.003 | 85.4 | 2.445 | 2.455 | 99.6 |
| 150 | 1.64E-04 | 1.61E-04 | 98.1 | 0.0025 | 0.00247 | 98.8 | 1.722 | 1.699 | 98.6 |

(a)　　　　　　　　　　　　　　　　(b)



(c)
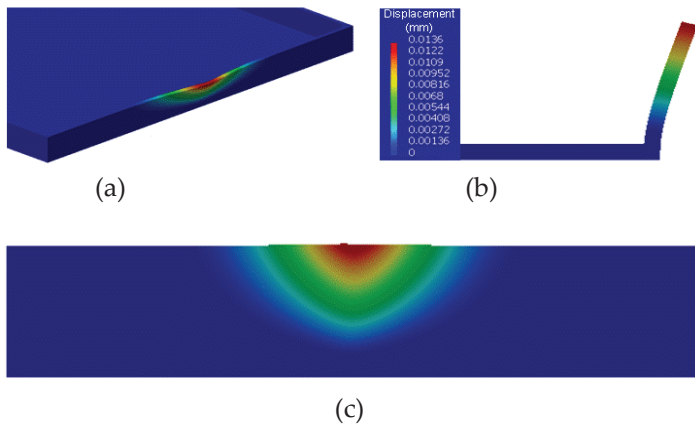
FIGURE 11: (a) Machining simulation for displacement analysis of the test part at the middle location of cutter feed. (b) Cut plane analysis of the part. (c) Back view of the part.

## 5.2 Multiple regression analysis

A set of 27 runs were generated from Section 3.2 to perform the regression analysis. Table 6 shows the training data set for the parameters and the displacements at five different locations along the cutter feed position. Assumptions of normality and independence of residuals were first checked using a normal probability and residual plot. The normal probability plot of the residuals for displacement at D1, D2, D3, D4 and D5 were shown in Figure 12. In this plot, the actual data are ranked and sorted, and an expected normal value is computed and compared with an actual normal value for each case. As shown in Fig. 12, the data are spread roughly along the straight line which indicates that the normal distribution of residuals was satisfied.
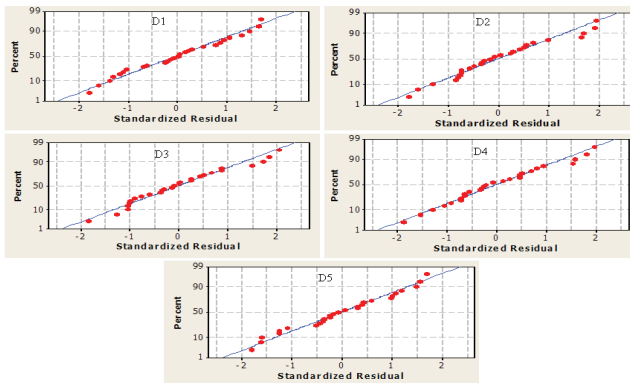


FIGURE 12: Normal probability of residuals for D1, D2, D3, D4 and D5.

TABLE 6: Training data set for regression analysis.

| SPEED (rpm) | FEED (mmpt) | RDOC (mm) | WP [t] (mm) | WP [h] (mm) | WP [l] (mm) | D1 (μm) | D2 (μm) | D3 (μm) | D4 (μm) | D5 (μm) |
|---|---|---|---|---|---|---|---|---|---|---|
| 4244 | 0.02 | 0.1 | 1.5 | 5 | 60 | 0.0835 | 0.6730 | 0.6770 | 0.6740 | 0.0783 |
| 4244 | 0.02 | 0.1 | 1.5 | 10 | 90 | 0.1060 | 2.6900 | 2.7300 | 2.6900 | 0.0935 |
| 4244 | 0.02 | 0.1 | 1.5 | 15 | 120 | 0.1230 | 6.5200 | 6.7300 | 6.5900 | 0.1060 |
| 4244 | 0.05 | 0.2 | 2 | 5 | 60 | 0.1240 | 0.7620 | 0.7670 | 0.7560 | 0.1290 |
| 4244 | 0.05 | 0.2 | 2 | 10 | 90 | 0.1540 | 2.7900 | 2.8200 | 2.7800 | 0.1360 |
| 4244 | 0.05 | 0.2 | 2 | 15 | 120 | 0.1750 | 6.6000 | 6.7500 | 6.6000 | 0.1480 |
| 4244 | 0.08 | 0.3 | 2.5 | 5 | 60 | 0.1470 | 0.6780 | 0.6850 | 0.6780 | 0.1474 |
| 4244 | 0.08 | 0.3 | 2.5 | 10 | 90 | 0.1830 | 2.3000 | 2.3200 | 2.2900 | 0.1540 |
| 4244 | 0.08 | 0.3 | 2.5 | 15 | 120 | 0.2040 | 5.2600 | 5.3800 | 5.2700 | 0.1640 |
| 4509 | 0.02 | 0.2 | 2.5 | 5 | 90 | 0.0596 | 0.3170 | 0.3170 | 0.3180 | 0.0598 |
| 4509 | 0.02 | 0.2 | 2.5 | 10 | 120 | 0.0712 | 1.0200 | 1.0200 | 1.0200 | 0.0642 |
| 4509 | 0.02 | 0.2 | 2.5 | 15 | 60 | 0.0784 | 1.1200 | 2.2600 | 1.1100 | 0.0678 |
| 4509 | 0.05 | 0.3 | 1.5 | 5 | 90 | 0.2500 | 1.6500 | 1.6400 | 1.6600 | 0.1900 |
| 4509 | 0.05 | 0.3 | 1.5 | 10 | 120 | 0.2880 | 6.7400 | 6.7700 | 6.7400 | 0.2300 |
| 4509 | 0.05 | 0.3 | 1.5 | 15 | 60 | 0.2840 | 9.4200 | 10.014 | 9.4320 | 0.2560 |
| 4509 | 0.08 | 0.1 | 2 | 5 | 90 | 0.1210 | 0.7800 | 0.7610 | 0.7810 | 0.1190 |
| 4509 | 0.08 | 0.1 | 2 | 10 | 120 | 0.1470 | 2.7600 | 2.7700 | 2.7700 | 0.1280 |
| 4509 | 0.08 | 0.1 | 2 | 15 | 60 | 0.1660 | 4.9200 | 6.3100 | 4.9200 | 0.1380 |
| 4774 | 0.02 | 0.3 | 2 | 5 | 120 | 0.0965 | 0.5550 | 0.5510 | 0.5540 | 0.0881 |
| 4774 | 0.02 | 0.3 | 2 | 10 | 60 | 0.1250 | 1.8300 | 2.0500 | 1.5000 | 0.0968 |
| 4774 | 0.02 | 0.3 | 2 | 15 | 90 | 0.1450 | 4.5400 | 4.9400 | 4.5500 | 0.1050 |
| 4774 | 0.05 | 0.1 | 2.5 | 5 | 120 | 0.0754 | 0.3860 | 0.3860 | 0.3860 | 0.0761 |
| 4774 | 0.05 | 0.1 | 2.5 | 10 | 60 | 0.0869 | 1.1100 | 1.2300 | 1.1100 | 0.0784 |
| 4774 | 0.05 | 0.1 | 2.5 | 15 | 90 | 0.0959 | 2.4200 | 2.8500 | 2.6400 | 0.0840 |
| 4774 | 0.08 | 0.2 | 1.5 | 5 | 120 | 0.2230 | 1.7640 | 1.7700 | 1.7600 | 0.2180 |
| 4774 | 0.08 | 0.2 | 1.5 | 10 | 60 | 0.2900 | 5.5000 | 7.2000 | 6.3000 | 0.2560 |
| 4774 | 0.08 | 0.2 | 1.5 | 15 | 90 | 0.3290 | 9.6800 | 11.015 | 9.7600 | 0.2820 |

Figure 13 shows plotting of the residuals in time order of data collection. The purpose of this graph is to check the independence assumption on the residuals. It is desired that the residual plot should contain no obvious patterns. From the graph it shows a tendency to have runs of positive and negative residuals indicate the existence of a certain correlation. Also the plot shows that the residuals are randomly dispersed in both positive and negative along the run which indicates, a linear regression model is appropriate for the data.
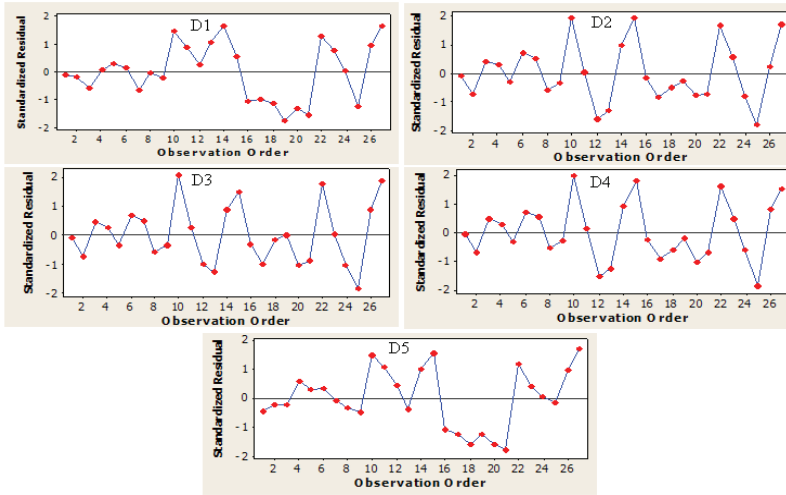
Figure 13: Residuals in time order for D1, D2, D3, D4 and D5.

Based on the validity of the assumptions, ANOVA was used for the regression analysis. From the ANOVA analysis, the R square obtained from the regression analysis for displacement at D1, D2, D3, D4 and D5 were 92.3%, 86.2%, 87.6%, 85.9% and 90.7% respectively, which indicated high correlation coefficient between the dependent variable and the predicted value. All these evidences showed a strong linear relationship between the predictor variables (*S, F, RDOC, WPT, WPH* and *WPL*) and the predicted variables.

The results of analysis of variance (ANOVA) of the models also supported strong linear relationship in the models (Table 7). The calculated F values of the regression were 39.80, 20.80, 23.52, 20.34 and 32.50, respectively. These high values indicated a great significance ($\alpha$ = 0.000) for the models in rejecting the null hypothesis ($H_o$) that every coefficient of the predictor variables in the model was zero. Instead, the alternative hypothesis, at least one of these coefficients did not equal to zero, was accepted. Therefore, the linear relationship between predicted variables and predictor variables significantly existed. The coefficients of all predictor variables and constants of the models are listed in Table 8. According to these coefficients, the multiple regression models for *D1, D2, D3, D4* and *D5* can be written as, respectively:

*D1 = 0.0005 + 0.000035S + 1.707F + 0.39878RDOC - 0.10834WPT + 0.004670WPH + 0.0000339WPL*

*D2 = 2.052 - 0.000102S + 26.624F + 5.952RDOC - 3.3362WPT + 0.47683WPH + 0.010356WPL*

*D3 = - 0.633 + 0.000657S + 31.672F + 5.503RDOC - 3.585WPT + 0.54291WPH + 0.00173WPL*

$D4 = 1.552 + 0.000049S + 28.746F + 5.618RDOC - 3.4204WPT + 0.48117WPH + 0.009648WPL$

$D4 = 0.0362 + 0.00002688S + 1.5672F + 0.29444RDOC - 0.09039WPT + 0.002717WPH - 0.0000469WPL$

TABLE 7: Analysis of variance (ANOVA).

| Model | Source | Sum of Squares | DF | Mean square | F | Sig. |
|-------|--------|---------------|----|-----|---|------|
| D1 | Regression | 0.140040 | 6 | 0.023340 | 39.80 | 0.000 |
|  | Residual | 0.011730 | 20 | 0.000586 |  |  |
|  | Total | 0.151770 | 26 |  |  |  |
|  | R-Square | 92.3 |  |  |  |  |
| D2 | Regression | 172.014 | 6 | 28.669 | 20.80 | 0.000 |
|  | Residual | 27.571 | 20 | 1.379 |  |  |
|  | Total | 199.585 | 26 |  |  |  |
|  | R-Square | 86.2 |  |  |  |  |
| D3 | Regression | 212.770 | 6 | 35.462 | 23.52 | 0.000 |
|  | Residual | 30.159 | 20 | 1.508 |  |  |
|  | Total | 242.928 | 26 |  |  |  |
|  | R-Square | 87.6 |  |  |  |  |
| D4 | Regression | 177.412 | 6 | 29.569 | 20.34 | 0.000 |
|  | Residual | 29.076 | 20 | 1.454 |  |  |
|  | Total | 206.488 | 26 |  |  |  |
|  | R-Square | 85.9 |  |  |  |  |
| D5 | Regression | 0.096431 | 6 | 0.016072 | 32.50 | 0.000 |
|  | Residual | 0.009890 | 20 | 0.000495 |  |  |
|  | Total | 0.106321 | 26 |  |  |  |
|  | R-Square | 90.7 |  |  |  |  |

TABLE 8: The model coefficients.

|  | D1 | D2 | D3 | D4 | D5 |
|--|----|----|----|----|----|
| *Constant* | 0.0005 | 2.052 | -0.633 | 1.552 | 0.03621 |
| *S* | 0.00003505 | -0.000102 | 0.000657 | 0.000049 | 0.00002688 |
| *F* | 1.7070 | 26.624 | 31.672 | 28.746 | 1.5672 |
| *RDOC* | 0.39878 | 5.952 | 5.503 | 5.618 | 0.29444 |
| *WPT* | -0.10834 | -3.3362 | -3.5850 | -3.4204 | -0.09039 |
| *WPH* | 0.004670 | 0.47683 | 0.54291 | 0.48117 | 0.002717 |
| *WPL* | 0.0000339 | 0.010356 | 0.001730 | 0.009648 | -0.0000469 |

## 6.0    CONCLUSIONS

Accuracy of machined components is one of the most critical considerations for many manufacturers especially in aerospace industry where most of the part used a thin-walled structure. In the current work, a new CAD/CAE/CAM integrated methodology for predicting

the surface errors when machining a thin-wall low rigidity component and the statistical analysis to determine the correlation between a criterion variable (form errors) and a combination of a predictor (cutting parameters and component attributes) were developed. A set of machining tests have been done in order to validate the accuracy of the model. A good agreement between simulation and experimental results show the validity of the proposed model in handling real-field problems. In addition, results from the statistical analysis showed a strong linear relationship between the predictor variables (*S, F, RDOC, WPT, WPH* and *WPL*) and the predicted variables (surface errors). Prediction of the surface errors due to the flexibility of the workpiece can be easily predicted with the proposed CAD/CAE/CAM integrated methodology. On the other hands, the advantages of the proposed model are for minimizing the analysis time i.e. integration between CAD/CAE/CAM, fast design-analysis loop, multidiscipline collaboration and the flexibility to create complex finite element models while maintaining associativity with the master design, thereby avoiding time-consuming and error-prone transfer of geometry. The CAD/CAE/CAM integrated methodology would be an efficient means for analysing the root cause of errors induced during machining of thin-wall parts and provide an input for downstream decision making on error compensation. To a large extent, through the CAD/CAE/CAM model, manufacturers can further enhance their productivity by eliminating the need of expensive preliminary cutting trials often require for validating the designed machining process plan.

## ACKNOWLEDGEMENTS

## REFERENCES

[1]     Songlin D, R. Izamshah R.A, John P.T Mo, Quansheng L., Online tool life prediction in the machining of titanium alloys, J. of Key Engineering Materials Vol. 458 (2011) 355-361.

[2]     M.A Elbestawi, R.Sagherian, Dynamics modelling for the prediction of surface errors in the milling of thin-walled sections, J. of Materials Processing Technology 25 (1991) 215-228.

[3]     E. Budak, Y. Altintas, Peripheral milling conditions for improved dimensional accuracy, Int. J. Mach. Tools Manuf. 34 (1994) 907-918.

[4]     J.W Sutherland, R.E DeVor, An improved method for cutting force and surface error prediction in flexile end milling system, ASME J. Eng. Ind. 108 (1986) 269-279.

[5]     J.W Sutherland, R.E DeVor, An improved method for cutting force and surface error prediction in flexile end milling system, ASME J. Eng. Ind. 108 (1986) 269-279.

[6]     J.S Tsai, C.L. Liao, Finite element modelling of static surface errors in the peripheral milling of thin-walled workpiece, J. of Materials Processing Technology 94 (1999) 235-246.

[7]     S. Ratchev, W.Huang, S.Liu, A.A Becker, Modelling and simulation environment for machining of low-rigidity components, J. of Materials Processing Technology 153-154 (2004) 67-73.

[8]     S. Ratchev, W.Huang, S.Liu, A.A Becker, Milling error prediction and compensation in machining of low-rigidity parts, Int. J. of Mach. Tools Manuf. 44 (2004) 1629-1641.

[9]     J.K Rai, P.Xirouchakis, Finite element method based machining simulation environment for analyzing part errors induced during milling of thin-walled components, Int. J. of Mach. Tools Manuf. 48 (2008) 629-643.

[10]    R. Izamshah R.A, John P.T Mo, Songlin D, Finite element analysis of machining thin-wall parts, J. of Key Engineering Materials Vol. 458 (2011) 283-288.

[11]    S. Ratchev, S.Liu, W.Huang, A.A Becker, A flexible force model for end milling of low-rigidity parts, Int. J. of Mach. Tools Manuf. 153-154 (2004) 134-138.

[12]    M. Wan, W.H. Zhang, G.H Qin, Z.P Wang, Strategies for error prediction and error control in peripheral milling of thin-walled workpiece, Int. J. of Mach. Tools Manuf. 48 (2008) 1366-1374.

[13]    W. Chen, J. Xue, D. Tang, H. Chen, S. Qu, Deformation prediction and error compensation in multilayer milling process for thin-walled parts, Int. J. of Mach. Tools Manuf. 49 (2009) 859-864.

[14]    M.C. Yoon, Y.G Kim, Cutting dynamic force of endmilling operation, J. of Materials Processing Technology 155-156 (2004) 1383-1389.

[15]    M. D. Gall, Joyce P. Gall, Walter R. Borg, Educational Research: An Introduction,(6th Edition), Longman, New York (1996).

[16]    E. Budak, Analytical models for high performance milling. Part 1: Cutting forces, structural deformations and tolerance integrity, Int. J. of Mach. Tools Manuf. 46 (2006) 1478-1488.

[17]    M. Wan, W.H. Zhang, G. Tan, G.H Qin, New cutting force modelling approach for flat end mill, Chinese. J. of Aeronautics 20 (2007) 282-288.

[18]   W.A Kline, R.E. DeVor, I.A. Shareef, The prediction of surface accuracy in end milling, ASME J. Eng. Ind. 104 (1982) 272-278.

[19]   W. A. Kline, R. E. DeVor, J. R. Lindberg, The prediction of cutting forces in end milling with application to conering cuts, Int. J. Mach. Tool Des. 22 (1982) 7-22.

[20]   X.P. Li, H.Z. Li, Theoretical modelling of cutting forces in helical end milling with cutter runout, Int. J. of Mech. Sciences 46 (2004) 1399-1414.

[21]   G. Petropoulos, N.M. Vaxevanidis, Modelling of surface finish in electro-discharge machining based upon statistical multi-parameter analysis, J. of Materials Processing Technology 155-156 (2004) 1247-1251.

[22]   J.T. Lin, D. Bhattacharyya, V. Kecman, Multiple regression and neural networks analyses in composites machining, J. of Composites Sci. and Tech. 63 (2003) 539-548.

[23]   S.H. Yeo, M. Rahman, Y.S. Wong, Towards enhancement of machinability data by multiple regression, J. of Mech. Working Tech. 19 (1989) 85-99.

[24]   Songlin D, R. Izamshah R.A, John P.T Mo, Yongwei Z., Chatter detection in high speed machining of titanium alloys, J. of Key Engineering Materials Vol. 458 (2011) 289-294.

[25]   W.S. Yun, D.W. Cho, An improved method for the determination of 3D cutting force coefficients and runout parameters in end milling, Int. J. of Adv Manuf. Tech. (2000) 16:851-858.